Published online 5 September 2011 *Nucleic Acids Research, 2011, Vol. 39, No. 22* ***9789–9802***
doi:10.1093/nar/gkr639

Cation binding to 15-TBA quadruplex DNA is a multiple-pathway cation-dependent process

Roman V. Reshetnikov[1,2], Jiri Sponer[3,*], Olga I. Rassokhina[4], Alexei M. Kopylov[4], Philipp O. Tsvetkov[5], Alexander A. Makarov[5] and Andrey V. Golovin[1,2,*]

[1]Department of Boiengineering and Bioinformatics, Lomonosov Moscow State University, GSP-1, Leninskie Gory, Moscow, 119991, [2]Apto-Pharm LLC, Kolomensky pr., 13A, Moscow, 115446, Russian Federation, [3]Institute of Biophysics, Academy of Sciences of the Czech Republic, Královopolská 135, 61265 Brno, Czech Republic, [4]Chemistry Department, Lomonosov Moscow State University, GSP-1, Leninskie Gory and [5]Engelhardt Institute of Molecular Biology, Russian Academy of Sciences, Moscow, 119991, Russian Federation

Received March 25, 2011; Revised July 19, 2011; Accepted July 22, 2011

ABSTRACT

A combination of explicit solvent molecular dynamics simulation (30 simulations reaching 4 μs in total), hybrid quantum mechanics/molecular mechanics approach and isothermal titration calorimetry was used to investigate the atomistic picture of ion binding to 15-mer thrombin-binding quadruplex DNA (G-DNA) aptamer. Binding of ions to G-DNA is complex multiple pathway process, which is strongly affected by the type of the cation. The individual ion-binding events are substantially modulated by the connecting loops of the aptamer, which play several roles. They stabilize the molecule during time periods when the bound ions are not present, they modulate the route of the ion into the stem and they also stabilize the internal ions by closing the gates through which the ions enter the quadruplex. Using our extensive simulations, we for the first time observed full spontaneous exchange of internal cation between quadruplex molecule and bulk solvent at atomistic resolution. The simulation suggests that expulsion of the internally bound ion is correlated with initial binding of the incoming ion. The incoming ion then readily replaces the bound ion while minimizing any destabilization of the solute molecule during the exchange.

INTRODUCTION

The ability of guanine-rich oligonucleotides to self-associate into polymers based on a G-quartet structure of four Hoogsteen-paired, coplanar guanines have been recognized for almost half a century (1). Guanine-rich segments, which have functional roles *in vivo*, were found in biologically significant regions of the genome such as telomeres (2–4) and immunoglobulin switch regions (5,6); potential quadruplex-forming promoter sequences have been located in a number of oncogenes and cancer-relevant genes (7–10). Nucleic acid quadruplexes (G-DNA) are also promising therapeutic agents: many RNA and DNA aptamers, identified for specific targets by *in vitro* selection techniques, form quadruplex structures (11–13). Therefore, structural stability and other aspects of physical chemistry of quadruplex DNA are important issues for the pharmacological industry and modern biology.

The formation and structural stability of G-quadruplexes depends on several factors, such as stacking interactions between nucleic acid bases, hydrogen bonds between them, electrostatic interactions and hydration shell. In addition to those typical for duplex DNA stabilizing factors, quadruplexes have also specific ones, namely, coordination of carbonyl oxygens by cations inside the G-DNA stems and presence of connecting single-stranded loops in monomeric and dimeric G-DNA molecules (14,15).

It was previously shown that length and sequence of loops have a strong influence on the G-quadruplex stability and folding efficiency (16–20), but full understanding of the rules driving the quadruplex folding is far from being achieved. It is also well-known that formation of quadruplexes requires the presence of cations (21–23). The location of the cations inside of the quadruplex structure depends on the cation size and charge. For example, Na^+ ions location was found to vary between two positions: being sandwiched by the quartets and in the plane of a quartet (24,25). Cations such as K^+ and NH_4^+ are too large to be in the second position, so that they tend to be situated symmetrically between two consecutive quartets (25–27). Majority of known quadruplex

*To whom correspondence should be addressed. Tel: +7 495 939 53 05; Fax: +7 495 939 31 81; Email: golovin@belozersky.msu.ru
Correspondence may also be addressed to Jiri Sponer. Tel: 420 541 517 133; Fax: 420 541 212 179; Email: sponer@ncbr.chemi.muni.cz

structures are obtained with the NMR method, which has limited capability to detect the bound ions. In general, the available experimental techniques do not provide much information about details of the structural dynamics of the ion binding to G-DNA.

Molecular dynamics (MD) simulation is a valuable tool for investigation of G-DNA structures (28–40). Recently, we have carried out a first microsecond scale (12 μs in total) explicit solvent MD simulation study on G-quadruplex, namely on thrombin-binding aptamer (15-TBA) (41). Current force fields, such as the parmbsc0 (42), provide good description of G-quadruplex structure stems. Capability of the simulations to quantitatively capture structural dynamics of the loops is, however, still rather limited (43). In addition, the classical force field MD simulation method treats only approximately some intra- and intermolecular interactions that can affect quadruplex stability and interactions between the G-DNA and the cations, although the overall picture of the ion–G-DNA binding is rather realistic (43).

Our preceding study on 15-TBA illustrated how loops can influence quadruplex geometry depending on their sequence, length and conformation. It was also shown that properly folded unimolecular G-quadruplex structure can be viable in the water solution without the stabilizing intrastem cations for a sufficiently long time to spontaneously capture a bulk cation (41). However, there are some contradictions about the final complex stoichiometry and cation location in 15-TBA structure in the available experimental studies (see below), which were not addressed in our previous work. Thus in this work we provide in-depth analysis specifically focusing on ion–15-TBA interactions. Besides specifically investigating 15-TBA our study reports several observations that give broader insights into the basic principles of interactions between monovalent cations and G-DNA molecules.

15-TBA forms intramolecular antiparallel guanine quadruplex. It consists of two stacked planar G-quartets (G-stem) that are connected with three lateral loops—two TT and one TGT (44) (Figure 1).

NMR study of the structure of 15-TBA in presence of Sr^{2+} revealed that the structural cation probably binds between the planes of quartets (the central binding site), being coordinated by eight O6 atoms of the guanines (45). In contrast, Marathias and Bolton (46,47) suggested 1:2 binding stoichiometry with two outer potassium-binding sites in the 15-TBA structure. One between the upper G-quartet and the TGT loop (the upper binding site) and the other under the lower G-quartet between the TT loops (the lower binding site).

In 2009, Plavec and colleagues (48) directly localized $^{15}NH_4^+$ cation-binding sites within the 15-TBA with the use of NMR and other spectroscopic methods. Given that 15-TBA G-quadruplex adopted the same topology in the presence of $^{15}NH_4^+$ as with K^+, the authors examined potential differences of the loops structures. All three loops adopted similar structures in the presence of $^{15}NH_4^+$ and K^+. Plavec *et al.* showed that NH_4^+ ion is bound to the central binding site. The signal from the lower binding site was 10 times weaker, while there was no NH_4^+ localization in the proximity of the TGT loop.

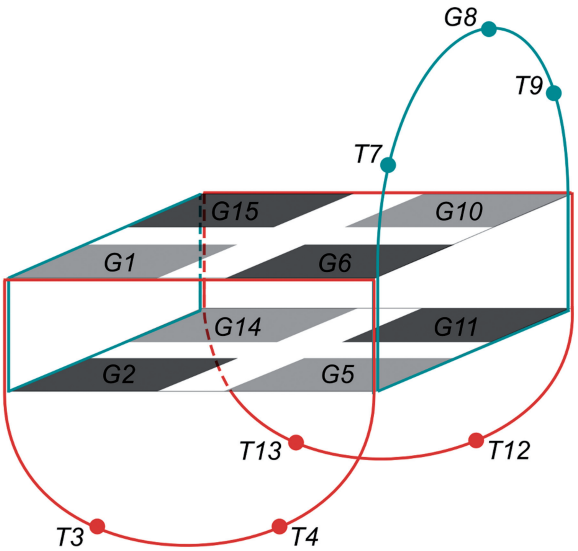

Figure 1. 15-TBA fold. Two G-quartets, upper (G1, G6, G10 and G15) and lower (G2, G5, G11 and G14), form G-quadruplex. Lighter and darker tetragons show *syn* and *anti* stem nucleotides. The remaining nucleotides form one TGT and two TT loops. An ~2-fold axis of symmetry relates the two halves of the G-quadruplex, resulting in two symmetric wide grooves (blue) and two symmetric narrow grooves (red).

Although this NH_4^+ experiment does not support the 1:2 binding pattern, we need to keep in mind that NH_4^+ and K^+ have markedly different interactions with the carbonyl oxygens of nucleic acids bases. NH_4^+ ion can form hydrogen and ionic bonds. This restricts the geometry of relative positions of acceptors and donors of H-bonds. K^+ cation can form coordination and electrostatic interactions with more variable geometry. In addition, it was shown with UV melting that HIV-1 integrase aptamer T30923 with similar topology as 15-TBA binds three potassium cations, presumably one between the quartets and the other two at the lower and upper binding sites (49). Therefore, stoichiometry of the complex between 15-TBA and potassium is still an open question.

We investigated the atomistic picture of ion binding to 15-TBA with combination of explicit solvent MD (30 new trajectories with aggregate length of 4 μs), hybrid quantum mechanics/molecular mechanics (QM/MM) approach and isothermal titration calorimetry (ITC). Our results indicate that there are three cation interaction sites in the structure of 15-TBA. However, two of them (the upper and lower binding sites) cannot keep the bound cation which is dominantly sucked by the central cation-binding site between the G-quartets. The TGT loop acts as a gate, which guides the cation to pass into the aptamer interior and helps to lock it in its final binding site.

Our study shows that cation-binding to 15-TBA is a surprisingly complex multiple pathway process whose atomistic details are greatly affected by the type of the cation. The results also suggest (at least for the two-quartet 15-TBA) that substantially pre-folded state of the quadruplex is necessary for cation binding. The cation stabilizes the folded 15-TBA structure and the simulations

indirectly indicate that the cation can also direct pre-folded structures to final conformation. The basic results obtained in the article should be valid also for other G-quadruplex structures.

MATERIALS AND METHODS

Classical MD simulations

We have carried out three sets of simulations. First, we have simulated the NMR structure of 15-TBA based on PDB entry 148d (44), eighth frame. Eight simulations were carried out in order to enhance the sampling using multiple-independent simulations; three with Na^+ cations and five with K^+ (Table 1). There were no cations initially placed inside the 15-TBA structure in these simulations.

Sodium is known as weak stabilizer of 15-TBA. Nevertheless, we decided to perform simulations with both K^+ and Na^+ ions. Description of cations by pair-additive force fields is imperfect (50). Specifically, the simple force field description underestimates the binding energy in the minimum and exaggerates the steepness of the repulsive part of the interaction energy curves compared to the QM reference data (43). Thus effective size of real potassium cation for direct ion–stem interactions would be somewhere between current parameters of sodium and potassium while the force field potassium looks to be too large.

In the second set of simulations, hypothetical model structure of TGT-free 15-TBA molecule was constructed from the NMR structure by deleting the TGT loop residues. There were eleven simulations in order to enhance the sampling, 1 with and 10 without the stabilizing cation initially inside the central binding site (Table 1).

In the third set, structure of TT-free 15-TBA molecule was modeled from the NMR structure by removing the TT loops residues and simulations analogous to those done for TGT-free 15-TBA were done (Table 1).

GROMACS 4.0 (51,52) software package was used for simulation and analysis of MD trajectories. Explicit solvent simulations in parmbsc0 force field (42) were performed at $T = 300\,K$ under control of velocity rescaling thermostat (53), with isotropic constant pressure boundary conditions under the control of the Berendsen algorithm of pressure coupling (54), and application of particle mesh Ewald (55) method for long-range electrostatics interactions (PME). A triclinic box of the TIP4P (56) water molecules was added around the DNA to a depth 15 Å on each side of the solute. Negative charges of systems were neutralized by adding of sodium or potassium cations, resulting in ~0.15 M concentration of the ions. In some simulations (Table 1) ~0.1 M of NaCl or KCl excess salt was added to the net-neutralizing ions. Sodium, potassium and chloride ions were added to the systems by replacing water molecules at random positions with minimal distance between ions equal to 6 Å. We used standard AMBER potassium (radius 0.2658 Å and well depth $0.00137\,kJ\,mol^{-1}$), sodium (radius 0.1868 Å, well depth $0.01589\,kJ\,mol^{-1}$) and chlorine (radius 0.2470 Å, well depth $0.41840\,kJ\,mol^{-1}$) parameters.

It is to be noted that in the course of our two KCl simulations salt-crystallization effect occurred. This is force field artifact caused by imbalance between water, cation and anion parameters (57). Thus, our excess salt KCl simulations are in fact closer to net-neutralizing K^+ conditions as the clustering tends to eliminate the added excess salt. However, we decided to not rerun the two affected KCl simulations with better balanced KCl parameters (57) for several reasons. The salt crystallization problem was not seen in the NaCl excess salt simulations, we did not see any visible difference in simulations run with net-neutral and excess salt conditions and the salt crystallization problem, even if it occurs, does not affect the remaining net-neutralizing ions. As we explained elsewhere, the cation binding to G-DNA is not expected to be significantly sensitive to details of cation parameters within the framework of the pair-additive force field approximation, i.e. the cation parameter sets available in the literature are assumed to perform similarly in this respect [see Figure 2 in Fadrna *et al.*'s article (43) and the pertinent discussion]. Note, that the effective size of the force field ion is also determined by the well depth, as the well depth and radius compensate for each other in the repulsive region.

Table 1. List of simulations

Simulated system and starting structure.	Trajectory length (ns)	Number of simulations	Quantity of atoms				
			DNA	Water (TIP4P)	K^+	Na^+	Cl^-
15-TBA without stabilizing cation in any binding site (ions: Na^+, Cl^-)	300	3	488	22 356	–	25	11
15-TBA without stabilizing cation in any binding site (ions: Na^+, Cl^-)	900[a]	1	488	22 356	–	25	11
15-TBA without stabilizing cation in any binding site (ions: K^+, Cl^-)	300	2	488	22 356	25	–	11
15-TBA without stabilizing cation in any binding site (ions: K^+)	300	3	488	22 444	14	–	–
TGT-free 15-TBA with stabilizing Na^+ in the central binding site (ions: Na^+, Cl^-)	300	1	390	26 540	–	29	19
TGT-free 15-TBA without stabilizing cation in any binding site (ions: Na^+, Cl^-)	60	10	390	26 536	–	29	19
TT-free 15-TBA with stabilizing Na^+ in the central binding site (ions: Na^+, Cl^-)	60	1	358	17 068	–	16	8
TT-free 15-TBA without stabilizing cation in any binding site (ions: Na^+, Cl^-)	60	10	358	17 068	–	16	8

[a]This simulation is described in our earlier study (41).

There have been two temperature coupling groups used in the simulations, the first consisting of DNA and the second consisting of water with ions.

QM/MM simulations

The starting conformations of 15-TBA were taken from PDB databank NMR structures, PDB ID 1c35 (47) for complexes with potassium and 1rde (45) for complex with barium. The later experimental structure was actually solved in the presence of strontium while there is no experimental structure available for 15-TBA with barium cation in the databank. However, it was shown by CD spectroscopy that barium and strontium form a very similar complex with the aptamer (58) and thus we decided to use the 1rde structure for simulation of complex between 15-TBA and Ba^{2+}. We prefer Ba^{2+} instead of Sr^{2+} to correlate QM/MM modeling and ITC experiments, because for the experiments we have chosen $BaCl_2$ since barium does not bio-accumulate (see the experimental part below).

Five systems were modeled (Figure 2).

Upper position of cation (systems 1 and 4) was calculated as an arithmetic mean value from potassium positions near the upper G-quartet (residues G1, G6, G10 and G15) from the structure 1c35. Central position (systems 2 and 5) is the geometrical center of the eight O6 atoms of the quaduplex-forming guanines. Lower position of cation (systems 3 and 4) was calculated as an arithmetic mean value from potassium positions near the lower G-quartet (residues G2, G5, G11 and G14) from the structure 1c35. Systems 1–4 were modeled with potassium and system 5 was modeled with barium. MM part was described with parameters of the parmbsc0 (42) force field. The QM system was described in terms of pseudopotential plane-wave implementation of density functional theory (59) (PW-DFT) with a spin polarized formalism (60) and PW91 functional (61). The interactions between valence electrons and ionic cores were described by ultrasoft VDB pseudopotential (62). QM part consisted of 15-TBA nucleic acid bases (except of T7) and potassium or barium ions. Partitioning of the systems to QM and MM parts was made across the *N*-glycosidic bonds with introduction of capping hydrogen atoms in order to saturate the dangling bonds. The total size of the QM system was 178 atoms (179 in case of system 4). Van der Waals interactions, which are poorly described by default DFT, were corrected with Grimme's analytical potential (63). Each simulated system was filled with water molecules represented by TIP4P model (56), while total charge was neutralized with Na^+ ions. Water and ions were equilibrated around the DNA–cation complexes by 100 ps classical MD simulation with restrained position of nucleic acid and the cation.

The prepared systems were subjected to QM/MM simulation with GROMACS/CPMD package (64) for 1.5 ps, with time step of 0.12 fs (~5 a.u.) and electronic mass 500. Temperature coupling with Nose-Hover (65,66) scheme allowed to observe behavior of systems at body temperature. Since we applied ultrasoft pseudopotentials, the basis set for the valence electrons consists of plane waves expanded up to a cutoff of 30 Ry. The QM subcell has cubic shape with 40 Ry side length which results in about 90 000 plane waves for wavefunction.

Isothermal titration calorimetry

The thermodynamic parameters of potassium and barium ions binding to d(GGTTGGTGTGGTTGG) and d(GGTTGGTCTGGTTGG) aptamers were measured using a iTC_{200} instrument (MicroCal, Northampton, MA, USA) as described previously (67). Experiments were carried out at 25°C in 20 mM Tris buffer, pH 6.8 in the presence of 140 mM LiCl. Two-microliter aliquots of KCl or $BaCl_2$ solution were injected into the 0.2 ml cell containing the DNA solution to achieve a complete binding isotherm. DNA concentration in the cell ranged from 50 to 250 μM and metal ions concentration in the syringe ranged from 1 to 10 mM. The heat of dilution was measured by injecting the ligand into the buffer solution; the values obtained were subtracted from the heat of reaction to obtain the effective heat of binding. The resulting titration curves were fitted using MicroCal Origin software. Affinity constants (K_a), binding stoichiometry (N) and enthalpy (H) were determined by a non-linear regression fitting procedure. Consequently, the entropy variations (ΔS) were calculated from the standard thermodynamic equations. ITC measurements for each aptamer have been repeated at least three times and yielded similar thermodynamic parameters.

RESULTS

Classical MD simulations

Probability and putative path of cation ingress into different ion-binding sites of 15-TBA were studied with MD in parmbsc0 force field. We have simulated the complete 15-TBA system in water solution in presence of excess salt NaCl, KCl and net-neutral K^+ ions (without Cl^-). In all cases the initial position of ions was random and

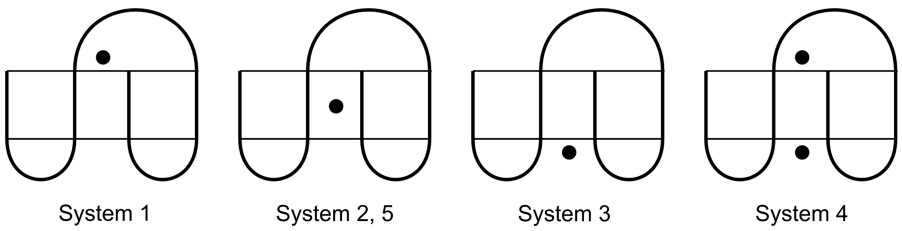

Figure 2. Variants of 15-TBA-cation complexes used in QM/MM computations.

no ion was initially present inside the quadruplex. In all eight simulations (cf. Table 1) the 15-TBA molecule spontaneously sucked a cation from the bulk which finally reached the central binding cavity. The initial pre-binding of the cation to the quadruplex is the rate-limiting step. One additional 15-TBA simulation that also revealed a swift capture of Na^+ is described elsewhere (41).

Sodium ion capture

Sodium cation has smaller radius than potassium (see 'Materials and Methods' section). Thus, it is sterically easier for sodium to find a way into the central binding site. In two cases out of three, the sodium initially bound with the upper binding site and in the remaining case it penetrated inside the 15-TBA through the pore between the TT loops. In the individual simulations, the initial binding of the sodium cation occurred at 1, 112 and 61 ns, respectively. The time spent by sodium at the upper binding site (including the time spent in plane of the G-quartet) was 1 and 4 ns while the cation spent 7 ns at the lower binding site.

Penetration of the cation into the central binding site from top of the structure requires several structural conditions (Figure 3). First, the G8 and T9 bases obstructing access to the inner cavity must realign to permit access to the O6 atoms of the upper quartet guanines. Second, the guanines composing the G-quartet must be separated to provide the cation sufficient access to bind the quartet plane. Then the cation can move to its final position inside the stem.

Dynamics of sodium cation entering the central binding site from the top of the 15-TBA structure is presented on the Figure 4. The space area between guanines of the upper quartet depends on the presence or absence of the cation inside the quadruplex. In this particular simulation, the cation penetrated into the central binding site at 112 ns of the trajectory. It became possible since the G8 base opened the upper gate for the ion to move inside (Figure 4, lower graph). The cation must traverse two gates, one of which is formed by the TGT loop and the other by the upper G-quartet. After ion uptake from the bulk the gates closed. The space between the guanines of the quartet decreased and stabilized (Figure 4, upper graph after 112 ns) and the same is true for the distance between the centers of mass of G8 base and the G-quadruplex (Figure 4, lower graph after 112 ns).

Similar processes occur in the structure of the 15-TBA when the cation penetrates inside through the bottom part of the molecule (Supplementary Data and Supplementary Figure S1).

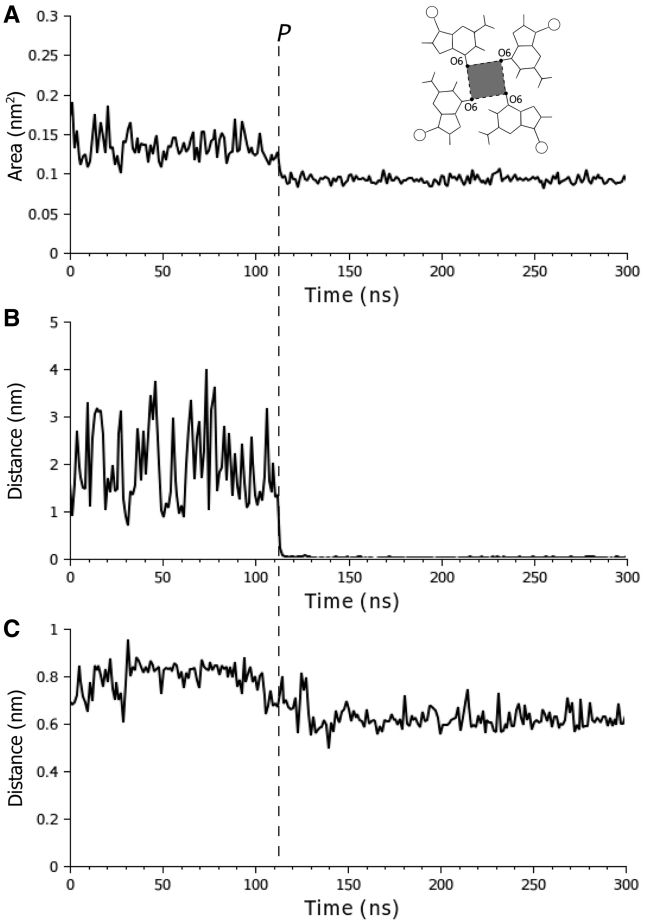

Figure 4. Structural dynamic of 15-TBA during the Na^+ cation penetration through the upper part of the structure. (**A**) Area of a tetragon formed by O6 atoms of the upper G-quartet. Sketch of the tetragon (gray) is depicted over the graph. (**B**) Distance between the Na^+ cation and center of mass (COM) of the eight O6 atoms of the G-quadruplex stem, i.e. the center of the quadruplex. (**C**) Distance between the COMs of the G8 nucleic acid base and the eight O6 atoms of the G-quadruplex stem. Similar graph for T9 is not shown. The letter 'P' and vertical dashed line mark the moment of the cation penetration into the quadruplex.

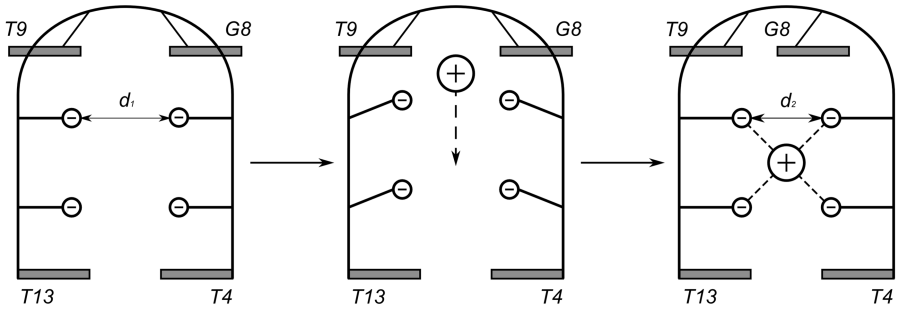

Figure 3. Sketch of ion penetration into the central binding site of 15-TBA through the top of the structure.

In order to get better insight into the details of the ion binding, we monitored the process of dehydration of the cation along its trajectory to the center of the quadruplex. This is described in the Supplementary Data, Supplementary Figures S2–S4 and the corresponding text.

Simulations with potassium

In the simulations of 15-TBA in a solution containing only net-neutralizing potassium cations, in two cases out of three the cation initially bound with the lower binding site. It occurred at 10 and 44 ns in the respective simulations. The cation subsequently spent 4 and 1 ns in the initial binding site, being then sucked by the central binding site.

In the third simulation, the aptamer did not capture the stabilizing cation from the solution till the 149 ns of the MD trajectory. At this time, the structure of the quadruplex started to collapse with G1 and G2 nucleic acid bases extruded from the G-stem (Figure 5). Then the potassium cation entered the quadruplex through the formed hole. It bound first at the upper binding site for ~1 ns and then it moved to the final position between the two G-quartets. The subsequent recovery of the 15-TBA structure required more time in the third simulation due to an interaction between G1 and T9 bases that occurred during the initial cation binding. The quadruplex structural recovery (at 156 ns) was incomplete with detectable perturbation of the upper G-quartet structure. There was a conformational change in G1 with rotation around the C3′–O3′ bond and a shift in the ε torsion angle from ~174° to 68° (Supplementary Data and Supplementary Figure S5). The quadruplex did not achieve full structural recovery before the end of the MD trajectory. Although our 300 ns simulations are long relative to most found in the literature, these simulations remain shorter in duration relative to most of the dynamic events occurring within molecules. However, we anticipate that the 15-TBA structure would be fully restored on a longer time scale.

The behavior of the two KCl 15-TBA simulations was consistent with the above results. In both simulations, there were structural alterations of 15-TBA anterior to the cation binding. In the first case, the G1 turned around the C3′–O3′ bond, with ε torsion angle changed from ~174° to ~74° (as in the simulation discussed above), which resulted in increase of the space area between the guanines of the upper quartet. So the second gate was open, but the first gate (the TGT loop) became closed after the cation went through it (Figure 6). The Figure 6 also shows that the main element that opens or closes the gates is the G8, whereas movements of the T9 nucleic acid base do not depend on whether the cation is inside the 15-TBA or not (Figure 6, gray line).

In the second KCl simulation, the aptamer did not bind any cation till the 129 ns. Then its structure again almost collapsed (Supplementary Data and Supplementary Figure S6). The G-stem was split into two parts and distance between them was ~10 Å. It resulted in a wide pore, which led into the central binding site of the aptamer, so it was easy for a potassium cation to penetrate directly between the planes of G-quartets (Supplementary Data and Supplementary Figure S6). After that the G-quadruplex amazingly fully restored its optimal structure in <1 ns and remained entirely stable during the rest of the simulation.

Impact of the loops into cation binding

The preceding simulations indicate that the TGT loop plays an important role in interactions with bulk cations. To further examine its role in cation binding we

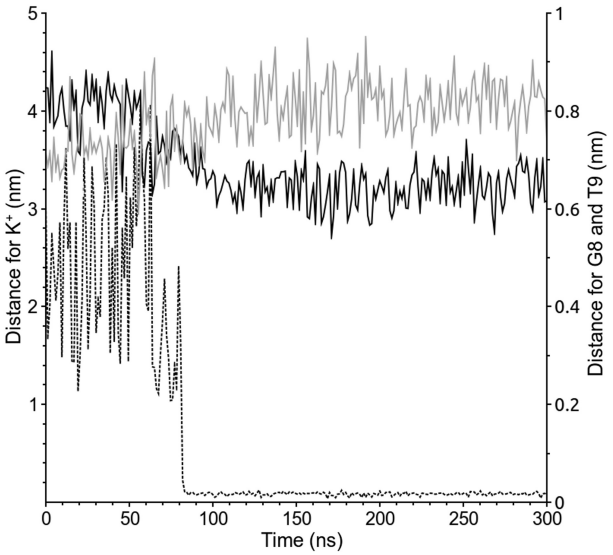

Figure 6. Behavior of the TGT loop during potassium cation uptake from the bulk. Dotted line: distance between COMs of the K^+ cation and the eight O6 atoms of the G-quadruplex stem. Solid black line: distance between COMs of the G8 nucleic base and the eight O6 atoms of the G-quadruplex. Solid gray line: distance between COMs of the T9 nucleobase and the eight O6 atoms of the G-quadruplex. Penetration of the cation into the G-stem (dotted line falls to 0 at 82 ns) correlates with G8 but not with T9 movement. The potassium cation did not spend any time in plane of the G-tetrad.

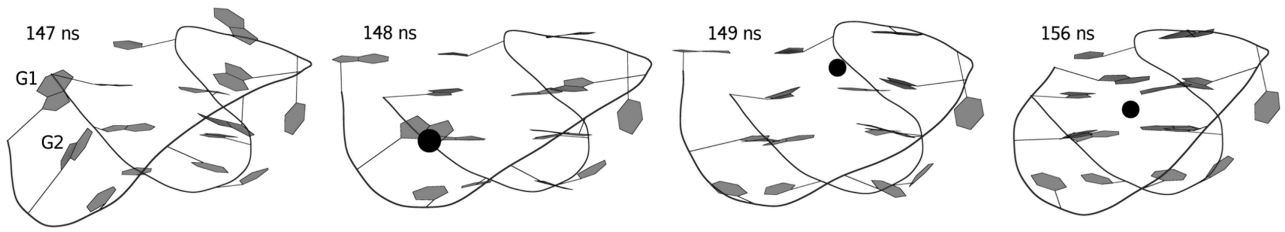

Figure 5. Penetration of potassium cation into substantially destabilized quadruplex.

performed test runs of 15-TBA without the TGT loop in NaCl water solution. There were 11 simulations, 1 with and 10 without the stabilizing sodium cation initially inside the central binding site.

In 4 simulations out of 10 the structure of the aptamer without the stabilizing cation collapsed during the first 10 ns of MD simulation, being unable to keep the G-quadruplex until a bulk cation is caught. When cation capture occurred at earlier simulation times (0–6 ns), the G-quadruplex was viable during rest of the 60 ns of MD trajectory, just as in case of the system with sodium cation initially placed into the G-quadruplex. Thus the TGT loop has major impact on the 15-TBA stability. On one hand, absence of the loop speeds up the spontaneous capture of the ion by the quadruplex, as the upper quartet is exposed to the bulk solvent. However, it also dramatically destabilizes the empty quadruplex. It appears that the second factor prevails, as the simulations show ~40% probability that the structure is completely lost before any cation can be retrieved from the bulk.

We then simulated 15-TBA without the TT loops in NaCl water solution. There were again 11 simulations, 1 with and 10 without the stabilizing sodium cation initially inside the central binding site. The G-quadruplex structure collapsed in only 2 of 10 simulations. If cation was captured, the systems were subsequently stable. The ion capture occurred between 2 and 6 ns in the individual simulations.

Notably, in these simulations of constructs lacking some of the loops, there were some transient but non-negligible events of bulk cation binding at the upper (seven times) or lower (five times) binding site in stable simulations with the central position already occupied by the structural cation. In most but not all cases, the second ion bound to the exposed quartet where the loop(s) were deleted. During these transient 1:2 biding events, due to electrostatic repulsion the ion trapped inside the stem shifted partially into the plane of the farther (with respect to the approaching ion) quartet. Statistics of the time periods for these binding events is given in the Supplementary Data, Supplementary Table S1. All these events finally ended up by releasing the outer cation back to the bulk solvent. The statistics can be used to roughly estimate the free energy difference between 1:1 and 1:2 complexes with one centrally bound ion, see Supplementary Data.

Analysis of the 300 ns trajectories of complete 15-TBA did not reveal any transient binding of second cation to quadruplex with occupied central ion position. However, in our earlier 900 ns 15-TBA simulation (41), there is one 55 ns and one 5 ns 1:2 binding event with the second ion bound in both cases at the lower 'TT loops' binding site, see Supplementary Data, Supplementary Table S1.

Besides the transient binding of the ions to the outer binding sites, we evidenced one event of full cation exchange between G-quadruplex of 15-TBA without TT loops and solution. At 45 ns of MD trajectory one of the bulk cations approached the upper binding site (Figure 7). Resultant repulsion between the two cations pushed the cation that was inside the G-stem out of the central binding site. For very short time of ~30 ps there has been 1:2 complex between DNA and the cations, very similar to that suggested by Marathias and Bolton (47). The incoming cation entered the central binding site and after additional 3.5 ns the lower (the originally bound) cation has been expelled into the solution.

To our best knowledge, it is the first occasion when spontaneous full exchange of a cation between G-DNA molecule and bulk solvent has been documented. In the preceding simulation and free energy studies (28–30), it was suggested that quadruplex molecules are basically never left vacant by cations. In addition, the studies suggested that folding/formation of quadruplex stems may proceeds via four-stranded intermediates with strand slippage and thus incomplete set of G-quartets while G-stem-like trimers and dimers are not viable. Once a single quartet is present in the structure it is already primarily stabilized by a cation (28). The present simulation adds another important insight into the overall picture. It appears that the likelihood, especially for short and slipped (28) stems with small number of complete quartets, to expel an internal ion into the solvent increases when a bulk cation is temporarily bound at the other side of the stem. The associated electrostatic repulsion between the lining-up cations leads to a partial relocation of the bound ions that promotes the expulsion. However, proximity of the bulk ion at the same time facilitates swift capture of the new ion, further reducing the likelihood that the stem is destabilized during the exchange (see 'Discussion' section).

QM/MM study

In the classical MD part of our study, the ions were sucked by the central binding site of 15-TBA after temporary binding either in the upper or lower binding site. However, MD cannot model polarization of electronic clouds, which adversely affects description of coordination interactions of ions with surrounding. That is why we decided to perform a QM/MM estimation of relative stability of different positions of K^+ within the quadruplex structure. Despite that QM/MM is limited by the affordable timescale it is an interesting independent test of the studied systems that complements classical MD.

Five systems (Figure 8) were constructed for QM/MM simulation: three systems with one K^+ cation in the upper, central or lower binding sites of the aptamer, another system containing two potassium cations within the aptamer (occupying the lower and upper sites), and one system with Ba^{2+} in the central binding site of the 15-TBA structure. Barium cation was chosen as a reference because it forms similar complexes with 15-TBA as a strontium, which is known to bind in the central site of the aptamer with 1:1 stoichiometry.

In both systems with potassium cation in the upper position (systems 1 and 4), the ion migrated toward the central binding site between the G-quartets. In the system 4, it was followed by expulsion of the K^+ cation from the lower binding position toward the bulk. In the system 3, the lower position proved to be unstable as well. The cation, after some fluctuations, also moved to the cavity

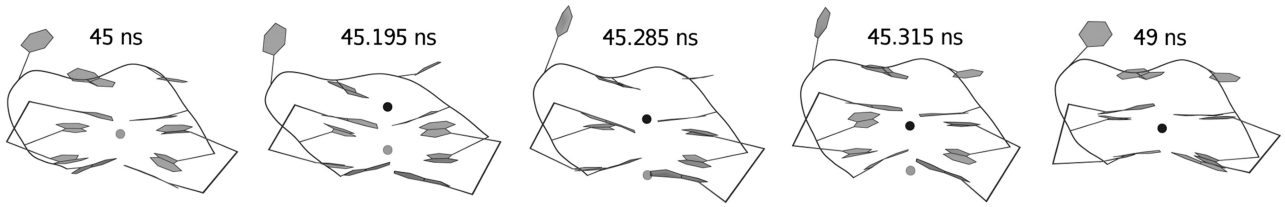

Figure 7. Complete exchange of sodium cation between the TT-free 15-TBA construct and bulk solution (snapshots are shown, the incoming and initially bound ions are shown as small black and gray dots, respectively).

center (Figure 8). Only systems with K^+ and Ba^{2+} cations initially placed into the central site (systems 2 and 5) showed stable ion positioning (Figure 8). During the simulation, the potassium performed periodical fluctuations within the cavity from location closer to the upper G-quartet to location closer to the lower one and back. In contrast, Ba^{2+} remained almost fixed in its position in the middle between the quartets. The first peak at 0.271 nm in the K^+–O6 pair radial distribution function (PRDF) is very similar to the relevant data of the study of solvation dynamics of K^+ in liquid methanol (68) (Supplementary Data and Supplementary Figure S7). Relative integration number for K^+ is 5.2. Position and coordination of Ba^{2+} are far more defined. PRDF has one peak with two maxima at 0.269 and 0.288 nm (Supplementary Data and Supplementary Figure S7). This is very close to relevant distances for 11-coordinate barium macrocycle complex and 8-coordinate complex of barium chloride with inositol (69). Integration number for the first peak from PRDF is exactly 8.

We have monitored the energy of the system during the QM/MM trajectory. The change of position of potassium cation toward central cavity of quadruplex during QM/MM simulation is clearly accompanied with optimization of relative total energy (see Supplementary Data, Supplementary Figure S8, Supplementary Tables S2 and S3 and the corresponding text).

There is remarkable difference between MD and QM/MM description of aptamer–cation interactions. The basic trend is similar, but the methods give different dynamics; in QM/MM it takes less than a picosecond for the cation to change its location from upper or lower binding site to the central one, whereas MD needs nanoseconds to move the ions. The difference arises from the methods limitations: MD cannot model electronic clouds shape and polarization; therefore, it considers only the long-range electrostatic part of aptamer-cation interactions. The simple Lennard-Jones Van der Waals potential is not optimal either, as already mentioned. QM/MM gives potentially more correct dynamics; however, we cannot rule out that the present results are considerably affected by approximations inherent to the QM/MM approach, less satisfactory relaxation and the very limited time scale. Further studies are needed to get a more converged picture. Nevertheless, the preliminary QM/MM calculations at least roughly show the expected direction in which the force field behavior deviates from eventual accurate electronic structure description.

Isothermal titration calorimetry

To clarify potassium coordination by thrombin-binding aptamer, thermodynamic parameters of potassium and barium interaction with 15-TBA were studied by ITC. A microcalorimetric approach allows the full characterization of this interaction in solution from thermodynamic point of view. At Figure 9 titration curves of K^+ and Ba^{2+} ions into 15-TBA solution are shown. It is obvious that Ba^{2+} has higher affinity ($1.1 \times 10^5\,M^{-1}$ against $5.0 \times 10^3\,M^{-1}$) and almost the same enthalpy of binding ($-9.7\,kcal\,mol^{-1}$ against $-8.2\,kcal\,mol^{-1}$) for aptamer as K^+. Fitting of binding isotherms with 'one-set-of-sites' model revealed that stoichiometry of both K^+ and Ba^{2+} binding is close to one. Refilling titration syringe with potassium after titration by barium (Figure 9, curve C) demonstrated the complete inhibition of K^+ binding (Figure 9, curve A).

Our MD study suggests that G8 base interferes with efficient shuffling of the ions into the stem cavity while it seems to stabilize the ion once bound by covering the stem entrance. Thus, replacement of G8 by smaller pyrimidine could make ion exchange between the G-quadruplex and bulk easier. To prove it the 15-TBA (G8)C mutant was synthesized and named as 15-TCT. The results of ITC of 15-TCT with barium and potassium in comparison with 15-TBA are given in Table 2. Indeed, 15-TCT experiences weak binding with potassium whereas barium binding is similar as for 15-TBA. We plan to investigate the role of the C8G substitution in the near future by simulation studies.

DISCUSSION AND CONCLUSIONS

Structural dynamics and stability of guanine quadruplex molecules are intimately interrelated with binding of monovalent ions inside the quadruplex stems and eventually at binding pockets created by single-stranded connecting loops. Despite limitations (31), molecular simulation technique can provide useful picture of ion binding to G-DNA complementing the experiments.

Recently, we have shown that properly pre-folded G-quadruplex structure (namely, thrombin-binding aptamer 15-TBA) in water solution without a cation inside its G-stem is viable for a sufficiently long time to spontaneously capture a bulk cation (41). However, the simulations predicted formation of 1:1 complex between 15-TBA and the ion, contrasting some studies suggesting 1:2 complex with vacant internal cavity of the quadruplex (46,47,70), with the ions located in the TGT and TT loop

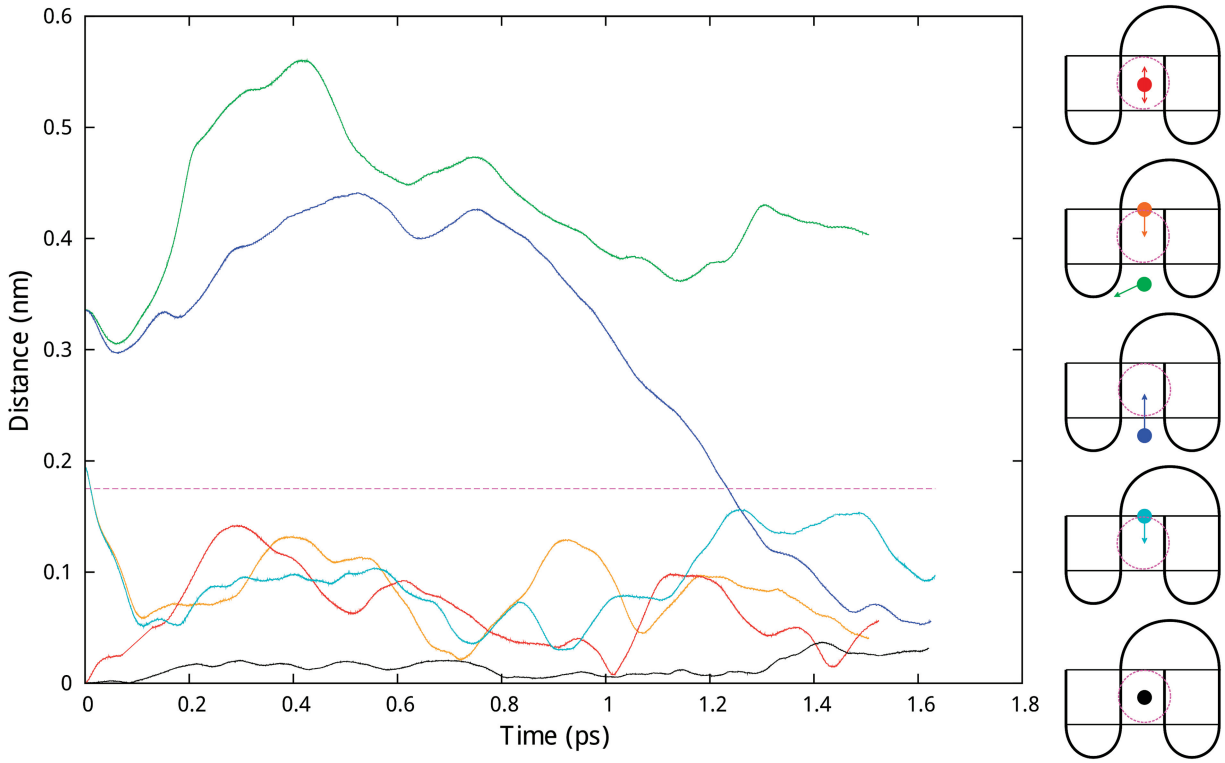

Figure 8. Behavior of the ions in different complexes with 15-TBA in the QM/MM MD runs. Left: the distance between the cation and geometrical center of the G-quadruplex. The border of the central binding site is denoted by the magenta dotted line; if the distance is between 0 and the border, then the cation is inside the central binding site. Right: schematic presentation of cation movements. Cation colors correspond to the distance chart.

regions. Here, we address this issue with a combination of explicit solvent MD (30 new individual trajectories with aggregate length of 4 μs), hybrid QM/MM approach and ITC measurements. Our study brings several new insights into G-DNA–cation interactions which are of general validity.

MD simulations do not support stable 1:2 complex between 15-TBA and the ions with empty central cavity

Our MD results indicate that there are three potential cation-binding sites in the 15-TBA molecule. One of them is the genuine site in the central cavity of the G-stem while the other sites are those outer sites considered by Marathias and Bolton at the stem–loop junctions. However, the simulations show that only the internal ion-binding site is stable. The upper and lower outer binding sites act as temporary ion traps for bulk cations, but they cannot retain the bound cation which is either quickly ingested by the central site or released back to the solvent if the central site is already occupied. The lower binding site is more populated than the upper. Based on our simulations, occupation probability for the lower site in case of the 1:2 binding is estimated to be 0.01–0.1 (see Supplementary Data for details). This value is close to that observed by Trajkovski *et al.* (48) for ammonium cation in NMR study. Therefore, 1:2 cation 15-TBA binding is predicted by simulations, but only for minor part of ensemble of molecules and basically always with the central binding site occupied by one of the ions. Our results are consistent with other experimental studies (48,71,72). It should be noted, however, that the difference between our results and the preceding literature suggesting the 1:2 binding is not insurmountable and can be explained by approximations of the individual approaches. First, there is no discrepancy regarding the solute geometry as we anyway firmly rely on experimental NMR geometries that behave stably in simulations. [Note that occasional incorrect experimental geometries usually lead to instabilities in simulations, as reported in the literature (29,41)]. The present simulations report some population of the 1:2 complexes, so these complexes are, in terms of free energy, relatively close to the 1:1 complex (see Supplementary Data for more details). Furthermore, as noted above and in the literature (31,43), the force field description of the ion–G-DNA interactions is not perfect. Imbalance in the force field could affect the calculated population of the 1:2 binding. In fact, the classical force fields underestimate binding of monovalent ions at the stem–loop junction of the diagonal loop $d(G_4T_4G_4)_2$ quadruplex (43). Considering this, the only remaining discrepancy would be the position of the ions in the 1:2 complexes. However, to predict the ion locations, the preceding studies relied primarily on simple molecular modeling rather than on direct experimental determination. The ion positions were predicted based on force field minimizations using simple distance-dependent dielectric constant method to mimic solvent screening and utilized the CHARMM force field. Compared to this

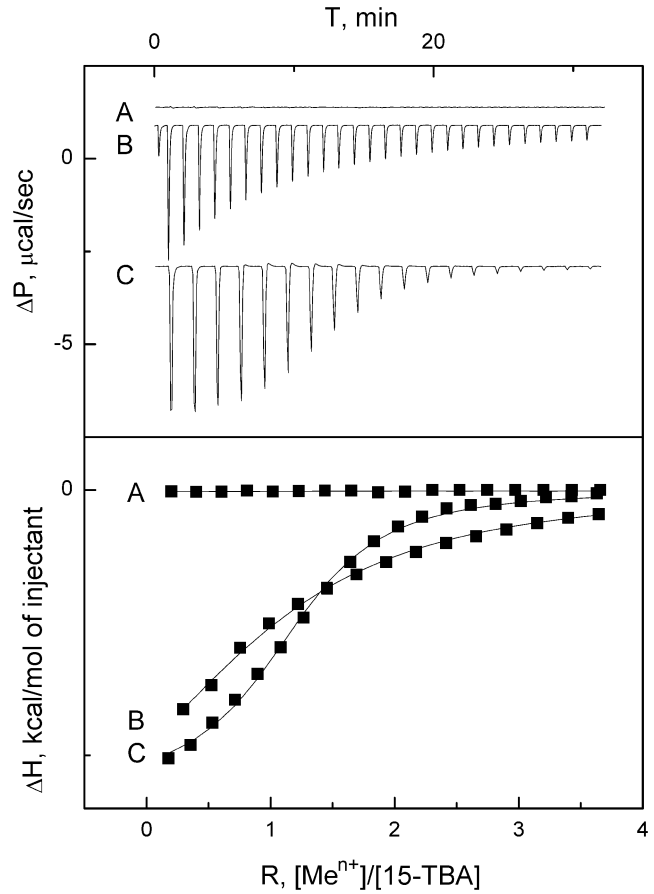

Figure 9. ITC curves of 15-TBA binding with potassium and barium. (**A**) Titration of 15-TBA by potassium after saturation with barium (competition), no effect; (**B**) binding of 15-TBA with potassium; (**C**) binding of 15-TBA with barium.

Table 2. Thermodynamics of binding of aptamers with ions[a]

Aptamer	Ion	K_a, M^{-1}	N, stoichiometry
125 μM 15-TBA	750 μM KCl	1.6×10^4	1
125 μM 15-TBA	750 μM $BaCl_2$	11×10^4	1:1
125 μM 15-TCT	750 μM KCl	Not detectable	–
250 μM 15-TCT	833 μM KCl	0.07×10^4	1
250 μM 15-TCT	833 μM $BaCl_2$	2.1×10^4	1:2

[a]Buffer: 140 mM LiCl, 20 mM Tris–HCl, pH 6.8.

approach, our extended explicit solvent simulation method is superior in accuracy. The distance-dependent dielectric constant approach is known to be inaccurate and often inverts the stability order compared to more physically based methods such as the Poisson-Boltzmann theory (73,74). In addition, the CHARMM force field has been reported to provide somewhat imperfect description of ion binding in G-DNA stems (43). Finally, in minimization runs the K^+ ions may have problems to enter the central cavity. As demonstrated in our simulations, very extensive thermal fluctuations of the quadruplex molecule are needed to allow the K^+ to penetrate into the G-DNA stem. In summary, we do not ultimately rule out the possibility of the 1:2 binding. However, based on our state-of-the art simulation approach, which is more advanced than the earlier computations could be, we rather predict that the central cavity of the G-DNA stem is always occupied by an ion.

MD simulations reveal details of the penetration of the ions into G-DNA

The simulations allowed us to obtain unique insights into the manner how the cations can penetrate into the 15-TBA structure. There are two gates from each side of the G-quadruplex that lead into the G-stem. The upper entrance is formed by the G8 base from the TGT loop (the first gate) and the space between guanine's O6 of the upper quartet (the second gate). The lower entrance is formed by non-canonical T–T pair from the bottom of the G-stem (the first gate) and the space generated by guanine's O6 from the lower quartet (the second gate). When there is no cation inside the molecule of the aptamer, all gates are open.

Once the ion is preliminarily captured by the 15-TBA molecule, its passage to the intrastem cavity is quick. When the quadruplex captures ion from the bulk, all gates tend to close (Figures 3, 4 and 6).

The loops are obviously not decisively important for the ion binding to G-DNA. However, they significantly modulate the ion-binding processes. The TGT loop plays at least three independent roles. First, it protects the 15-TBA structure from collapse in absence of the ion, as we have seen ~40% probability of loss of the structure when the TGT loop was deleted and stem ion absent. At the same time, the TGT loop slows down the initial ion binding since it partially obstructs the stem entrance. Thus, ion-free 15-TBA construct lacking the loop can more quickly capture the ion but is prone to swift disintegration. Finally, once the ion is inside the stem, the loop (mainly its G8 base) helps to keep the ion inside. Therefore, the net contribution from the TGT loop is overwhelmingly stabilizing.

Correlation of ion movement during full exchange of ion between G-DNA and bulk solvent

We report the first atomistic simulation capturing a complete spontaneous exchange of an ion bound inside the G-DNA stem with a bulk ion (Figure 7), in one of the simulations with the construct lacking the bottom TT loops. The ion expulsion occurred through the bottom part of the structure and was facilitated by approach of another ion from the other side of the stem (i.e. through the TGT outer binding site). The bulk ion (transiently bound in the TGT outer binding site) occupied the central cavity of the stem immediately after the originally bound ion left the area. Due to this correlation between transient ion binding and stem ion release, the stem was basically not left vacant by the ions. This indicates that probably vast majority of G-DNA ion exchange events can occur without any stem destabilization even for the two-quartet stem. The correlation between binding of bulk cation and expulsion of stem cation can greatly help to

protect short stems as well as kinetics intermediates with shifted strands during G-DNA folding/formation processes. When assuming participation of approaching bulk ions in the exchange (as seen in Figure 7), molecule with N consecutive quartets can release any internally bound ion in a stepwise manner via intermediates with N-1 bound ions (Supplementary Data and Supplementary Figure S9). The effect is likely less important for longer complete stems such as four-quartet stems. Four-quartet stem is very stable even with just two ions inside. It could smoothly exchange any intrastem ion through sequence of intermediates having at least two intrastem-bound ions even with entire separation between the individual ion release and ion-binding events (28,29).

Preliminary QM/MM simulations

Primary recognition of a cation by the upper or lower binding site can be described in terms of electrostatic interactions. However, ion interactions are more complex and are only approximately described by a classical MM utilized in MD simulations (43). Therefore, possible coordination part of the cation–aptamer interactions is not considered. Hybrid QM/MM simulation is a known technique to study ion-biopolymer complexes that provides reasonable speed with satisfactory accuracy (75–77). Due to enormous computer demands, QM/MM simulation trajectory at present is restricted by picoseconds range. This sampling time is definitely not enough to observe equilibration of system with initial geometry being far from the equilibrium state. However, a few picoseconds can provide at least some rough test of the ion interactions within the structure.

With the QM/MM method we examined steadiness of potassium cation localization in the three binding sites. The calculations supported MD results, and also indicated that the 1:2 stoichiometry of the complex is not likely; one of the cations in the 1:2 complex was displaced towards the bulk. So it is very likely that stoichiometry of complex between potassium and 15-TBA is 1:1 and that potassium locates in the central binding site of the aptamer, between two G-quartets, being associated with the O6 atoms of the quartet guanines by electrostatic and coordination interactions. To confirm it, we chose barium cation for a comparison. Ba^{2+} has the similar size and a charge as strontium while CD spectra of 15-TBA with Ba^{2+} and Sr^{2+} are almost superimposable (58). Stoichiometry of the complex between strontium and 15-TBA is 1:1 and the cation is very likely bound between the G-quartets.

ITC measurements

Our ITC measurements indicate that stoichiometry of the complexes between 15-TBA and barium or potassium is close to 1:1, moreover, competition study revealed that the cations occupy the same binding site. These results are entirely consistent with the simulations.

Multipathway processes are likely to participate in structural dynamics and folding of G-DNA molecules

Our results also shed the light on the question of what is primary—folding of the G-quadruplex structure with the following capture of the stabilizing cation, or assembling of the G-quadruplex structure around the cation. Properly folded 15-TBA lacking the bound ion proved to be viable in a timescale of several hundreds of nanoseconds, which is enough to meet and capture a cation (in ~0.1–0.2 M solutions used in simulations, see 'Materials and Methods' section). It was experimentally shown that 15-TBA can form unimolecular G-quadruplex structure at low temperatures in the solutions that are free of possible stabilizing cations (78). We suggest that there are constantly complex and variable folding–unfolding processes of G-quadruplex structures in water solution of 15-TBA at a room temperature, and addition of potassium only shifts the equilibrium in the solution. Therefore, cation is rather the stabilizer of the folded or pre-folded structure but not the initiator of folding. Note that although such processes are beyond the present simulation time scale, we also assume (as for the ion insertions into the quadruplex visualized in this study) that the actual folding process is realized via a rich stochastic spectrum of individual and diverse folding routes and attempts. The different microroutes (their probabilities) may differentially respond to changes of the external conditions and base sequence.

Complexity of structural rearrangements of G-DNA molecules can be illustrated for the ion-capture process by 15-TBA investigated in this study. In our extended set of simulations of either complete 15-TBA or its constructs lacking some of the loops, we observed altogether 23 individual events of penetration of the initially bulk cation into the central ion-binding position. We have evidenced diverse routes of cation penetration into the G-DNA molecule with a marked difference between the Na^+ and larger K^+ (Figures 3–6 and Supplementary Figure S6). Our simulations show that even such a simple process as capture of an ion by a G-DNA molecule is a complex multi-pathway process. Competition between the pathways may be strongly dependent on the type of the cation. We suggest that, in general, all processes that participate in G-DNA molecule folding could have very complex multiple-pathway nature, unique for each G-DNA sequence and fold. It would be very difficult to exhaustively capture this picture by the experimental techniques, as it would require nanosecond time resolution and atomistic spatial resolution of the solute geometries and ion positions. The method would have to reach at least millisecond time scale. Thus, despite their limitations, extended MD simulations can in future provide useful insights into the competition of micropathways between various experimentally detected substates occurring during folding and rearrangements of G-DNA molecules.

SUPPLEMENTARY DATA

Supplementary Data are available at NAR Online.

ACKNOWLEDGEMENTS

Computer resources were provided by the Research Computing Center of Moscow State University. The supercomputer, 'Chebyshev', was used for all modeling studies.

FUNDING

Funding for open access charge: Russian Foundation for Basic Research grant (11-04-02084-a); Ministry of Education and Science of Russian Federation grant (16.512.11.2009); Molecular and Cellular Biology Program of the Russian Academy of Sciences; Grant Agency of the Academy of Sciences of the Czech Republic (CR) grant (IAA400040802 to J.S.); Grant Agency of the CR grants (203/09/1476, P208/11/1822); Ministry of Education of the CR LC06030 and Academy of Sciences of the CR grants (AV0Z50040507, AV0Z50040702).

Conflict of interest statement. None declared.

REFERENCES

1. Gellert,M., Lipsett,M.N. and Davies,D.R. (1962) Helix formation by guanylic acid. *Proc. Natl Acad. Sci. USA*, **48**, 2013–2018.
2. Blackburn,E.H. (1994) Telomeres: no end in sight. *Cell*, **77**, 621–623.
3. De Lange,T. (2005) Telomere-related genome instability in cancer. *Cold Spring Harb. Symp. Quant. Biol.*, **70**, 197–204.
4. De Cian,A., Lacroix,L., Douarre,C., Temime-Smaali,N., Trentesaux,C., Riou,J.-F. and Mergny,J.-L. (2008) Targeting telomeres and telomerase. *Biochimie*, **90**, 131–155.
5. Sen,D. and Gilbert,W. (1988) Formation of parallel four-stranded complexes by guanine-rich motifs in DNA and its implications for meiosis. *Nature*, **334**, 364–366.
6. Simonsson,T. (2001) G-quadruplex DNA structures–variations on a theme. *Biol. Chem.*, **382**, 621–628.
7. Cogoi,S. and Xodo,L.E. (2006) G-quadruplex formation within the promoter of the KRAS proto-oncogene and its effect on transcription. *Nucleic Acids Res.*, **34**, 2536–2549.
8. Rankin,S., Reszka,A.P., Huppert,J., Zloh,M., Parkinson,G.N., Todd,A.K., Ladame,S., Balasubramanian,S. and Neidle,S. (2005) Putative DNA quadruplex formation within the human c-kit oncogene. *J. Am. Chem. Soc.*, **127**, 10584–10589.
9. Dexheimer,T.S., Sun,D. and Hurley,L.H. (2006) Deconvoluting the structural and drug-recognition complexity of the G-quadruplex-forming region upstream of the bcl-2 P1 promoter. *J. Am. Chem. Soc.*, **128**, 5404–5415.
10. Siddiqui-Jain,A., Grand,C.L., Bearss,D.J. and Hurley,L.H. (2002) Direct evidence for a G-quadruplex in a promoter region and its targeting with a small molecule to repress c-MYC transcription. *Proc. Natl Acad. Sci. USA*, **99**, 11593–11598.
11. Métifiot,M., Leon,O., Tarrago-Litvak,L., Litvak,S. and Andréola,M.-L. (2005) Targeting HIV-1 integrase with aptamers selected against the purified RNase H domain of HIV-1 RT. *Biochimie*, **87**, 911–919.
12. Bates,P.J., Kahlon,J.B., Thomas,S.D., Trent,J.O. and Miller,D.M. (1999) Antiproliferative Activity of G-rich Oligonucleotides Correlates with Protein Binding. *J. Biol. Chem.*, **274**, 26369–26377.
13. Bock,L.C., Griffin,L.C., Latham,J.A., Vermaas,E.H. and Toole,J.J. (1992) Selection of single-stranded DNA molecules that bind and inhibit humanthrombin. *Nature*, **355**, 564–566.
14. Lane,A.N., Chaires,J.B., Gray,R.D. and Trent,J.O. (2008) Stability and kinetics of G-quadruplex structures. *Nucleic Acids Res.*, **36**, 5482–5515.
15. Burge,S., Parkinson,G.N., Hazel,P., Todd,A.K. and Neidle,S. (2006) Quadruplex DNA: sequence, topology and structure. *Nucleic Acids Res.*, **34**, 5402–5415.
16. Smirnov,I. and Shafer,R.H. (2000) Effect of loop sequence and size on DNA aptamer stability. *Biochemistry*, **39**, 1462–1468.
17. Hazel,P., Huppert,J., Balasubramanian,S. and Neidle,S. (2004) Loop-length-dependent folding of G-quadruplexes. *J. Am. Chem. Soc.*, **126**, 16405–16415.
18. Smargiasso,N., Rosu,F., Hsia,W., Colson,P., Baker,E.S., Bowers,M.T., De Pauw,E. and Gabelica,V. (2008) G-quadruplex DNA assemblies: loop length, cation identity, and multimer formation. *J. Am. Chem. Soc.*, **130**, 10208–10216.
19. Guédin,A., Gros,J., Alberti,P. and Mergny,J.-L. (2010) How long is too long? Effects of loop size on G-quadruplex stability. *Nucleic Acids Res.*, **38**, 7858–7868.
20. Risitano,A. and Fox,K.R. (2004) Influence of loop size on the stability of intramolecular DNA quadruplexes. *Nucleic Acids Res.*, **32**, 2598–2606.
21. Pinnavaia,T.J., Marshall,C.L., Mettler,C.M., Fisk,C.L., Miles,H.T. and Becker,E.D. (1978) Alkali metal ion specificity in the solution ordering of a nucleotide, 5'-guanosine monophosphate. *J. Am. Chem. Soc.*, **100**, 3625–3627.
22. Chen,F.M. (1992) Strontium(2+) facilitates intermolecular G-quadruplex formation of telomeric sequences. *Biochemistry*, **31**, 3769–3776.
23. Smirnov,I. and Shafer,R.H. (2000) Lead is unusually effective in sequence-specific folding of DNA. *J. Mol. Biol.*, **296**, 1–5.
24. Phillips,K., Dauter,Z., Murchie,A.I., Lilley,D.M. and Luisi,B. (1997) The crystal structure of a parallel-stranded guanine tetraplex at 0.95 A resolution. *J. Mol. Biol.*, **273**, 171–182.
25. Ida,R. and Wu,G. (2008) Direct NMR detection of alkali metal ions bound to G-quadruplex DNA. *J. Am. Chem. Soc.*, **130**, 3590–3602.
26. Sket,P. and Plavec,J. (2010) Tetramolecular DNA quadruplexes in solution: insights into structural diversity and cation movement. *J. Am. Chem. Soc.*, **132**, 12724–12732.
27. Hud,N.V., Schultze,P., Sklenář,V. and Feigon,J. (1999) Binding sites and dynamics of ammonium ions in a telomere repeat DNA quadruplex. *J. Mol. Biol.*, **285**, 233–243.
28. Štefl,R., Cheatham,T.E., Špačková,N., Fadrná,E., Berger,I., Koča,J. and Šponer,J. (2003) Formation pathways of a guanine-quadruplex DNA revealed by molecular dynamics and thermodynamic analysis of the substates. *Biophys. J.*, **85**, 1787–1804.
29. Špačková,N., Berger,I. and Šponer,J. (1999) Nanosecond molecular dynamics simulations of parallel and antiparallel guanine quadruplex DNA molecules. *J. Am. Chem. Soc.*, **121**, 5519–5534.
30. Špačková,N., Berger,I. and Šponer,J. (2001) Structural dynamics and cation interactions of DNA quadruplex molecules containing mixed guanine/cytosine quartets revealed by large-scale MD simulations. *J. Am. Chem. Soc.*, **123**, 3295–3307.
31. Šponer,J. and Špačková,N. (2007) Molecular dynamics simulations and their application to four-stranded DNA. *Methods*, **43**, 278–290.
32. Li,M.-H., Zhou,Y.-H., Luo,Q. and Li,Z.-S. (2010) The 3D structures of G-quadruplexes of HIV-1 integrase inhibitors: molecular dynamics simulations in aqueous solution and in the gas phase. *J. Mol. Model*, **16**, 645–657.
33. Cavallari,M., Calzolari,A., Garbesi,A. and Di Felice,R. (2006) Stability and migration of metal ions in G4-wires by molecular dynamics simulations. *J. Phys. Chem. B*, **110**, 26337–26348.
34. Cavallari,M., Garbesi,A. and Di Felice,R. (2009) Porphyrin intercalation in G4-DNA quadruplexes by molecular dynamics simulations. *J. Phys. Chem. B*, **113**, 13152–13160.
35. Hazel,P., Parkinson,G.N. and Neidle,S. (2006) Predictive modelling of topology and loop variations in dimeric DNA quadruplex structures. *Nucleic Acids Res.*, **34**, 2117–2127.
36. Rueda,M., Luque,F.J. and Orozco,M. (2006) G-quadruplexes can maintain their structure in the gas phase. *J. Am. Chem. Soc.*, **128**, 3608–3619.

37. Li,H., Cao,E.-hua and Gisler,T. (2009) Force-induced unfolding of human telomeric G-quadruplex: a steered molecular dynamics simulation study. *Biochem. Biophys. Res. Commun.*, **379**, 70–75.
38. Pagano,B., Mattia,C.A., Cavallo,L., Uesugi,S., Giancola,C. and Fraternali,F. (2008) Stability and cations coordination of DNA and RNA 14-mer G-quadruplexes: a multiscale computational approach. *J. Phys. Chem. B*, **112**, 12115–12123.
39. Haider,S. and Neidle,S. (2010) Molecular modeling and simulation of G-quadruplexes and quadruplex-ligand complexes. *Methods Mol. Biol.*, **608**, 17–37.
40. Petraccone,L., Garbett,N.C., Chaires,J.B. and Trent,J.O. (2010) An integrated molecular dynamics (MD) and experimental study of higher order human telomeric quadruplexes. *Biopolymers*, **93**, 533–548.
41. Reshetnikov,R., Golovin,A., Spiridonova,V., Kopylov,A. and Šponer,J. (2010) Structural dynamics of thrombin-binding DNA aptamer d(GGTTGGTGTGGTTGG) quadruplex DNA studied by large-scale explicit solvent simulations. *J. Chem. Theory Comput.*, **6**, 3003–3014.
42. Pérez,A., Marchán,I., Svozil,D., Sponer,J., Cheatham,T.E., Laughton,C.A. and Orozco,M. (2007) Refinement of the AMBER force field for nucleic acids: improving the description of α/γ conformers. *Biophys. J.*, **92**, 3817–3829.
43. Fadrná,E., Špačková,N., Sarzyńska,J., Koča,J., Orozco,M., Cheatham,T.E., Kulinski,T. and Šponer,J. (2009) Single stranded loops of quadruplex DNA as key benchmark for testing nucleic acids force fields. *J. Chem. Theory Comput.*, **5**, 2514–2530.
44. Schultze,P., Macaya,R.F. and Feigon,J. (1994) Three-dimensional Solution Structure of the Thrombin-binding DNA Aptamer d(GG TTGGTGTGGTTGG). *J. Mol. Biol.*, **235**, 1532–1547.
45. Mao,X., Marky,L.A. and Gmeiner,W.H. (2004) NMR structure of the thrombin-binding DNA aptamer stabilized by Sr^{2+}. *J. Biomol. Struct. Dyn.*, **22**, 25–33.
46. Marathias,V.M. and Bolton,P.H. (1999) Determinants of DNA quadruplex structural type: sequence and potassium binding. *Biochemistry*, **38**, 4355–4364.
47. Marathias,V.M. and Bolton,P.H. (2000) Structures of the potassium-saturated, 2:1, and intermediate, 1:1, forms of a quadruplex DNA. *Nucleic Acids Res.*, **28**, 1969–1977.
48. Trajkovski,M., Šket,P. and Plavec,J. (2009) Cation localization and movement within DNA thrombin binding aptamer in solution. *Org. Biomol. Chem.*, **7**, 4677.
49. Jing,N., Marchand,C., Liu,J., Mitra,R., Hogan,M.E. and Pommier,Y. (2000) Mechanism of inhibition of HIV-1 integrase by G-tetrad-forming oligonucleotides in Vitro. *J. Biol. Chem.*, **275**, 21460–21467.
50. Cordomì,A., Edholm,O. and Perez,J.J. (2009) Effect of Force Field Parameters on Sodium and Potassium Ion Binding to Dipalmitoyl Phosphatidylcholine Bilayers. *J. Chem. Theory Comput.*, **5**, 2125–2134.
51. van der Spoel,D., Lindahl,E., Hess,B., Groenhof,G., Mark,A.E. and Berendsen,H.J.C. (2005) GROMACS: fast, flexible, and free. *J. Comput. Chem.*, **26**, 1701–1718.
52. Hess,B., Kutzner,C., van der Spoel,D. and Lindahl,E. (2008) GROMACS 4: algorithms for highly efficient, load-balanced, and scalable molecular simulation. *J. Comput. Chem.*, **4**, 435–447.
53. Bussi,G., Donadio,D. and Parrinello,M. (2007) Canonical sampling through velocity rescaling. *J. Chem. Phys.*, **126**, 014101–014107.
54. Berendsen,H.J.C., Postma,J.P.M., van Gunsteren,W.F., DiNola,A. and Haak,J.R. (1984) Molecular dynamics with coupling to an external bath. *J. Chem. Phys.*, **81**, 3684–3690.
55. Darden,T., York,D. and Pedersen,L. (1993) Particle mesh Ewald: An N•log(N) method for Ewald sums in large systems. *J. Chem. Phys.*, **98**, 10089–10092.
56. Jorgensen,W.L., Chandrasekhar,J., Madura,J.D., Impey,R.W. and Klein,M.L. (1983) Comparison of simple potential functions for simulating liquid water. *J. Chem. Phys.*, **79**, 926–935.
57. Joung,I.S. and Cheatham. (2008) Determination of alkali and halide monovalent ion parameters for use in explicitly solvated biomolecular simulations. *J. Phys. Chem. B*, **112**, 9020–9041.
58. Kankia,B.I. and Marky,L.A. (2001) Folding of the thrombin aptamer into a G-quadruplex with Sr(2+): stability, heat, and hydration. *J. Am. Chem. Soc.*, **123**, 10799–10804.
59. Payne,M., Teter,M., Allan,D., Arias,T. and Joannopoulos,J. (1992) Iterative minimization techniques for ab initio total-energy calculations: molecular dynamics and conjugate gradients. *Rev. Mod. Phys.*, **64**, 1045.
60. Pant,M.M. and Rajagopal,A.K. (1972) Theory of inhomogeneous magnetic electron gas. *Solid State Commun.*, **10**, 1157–1160.
61. Perdew,J.P., Chevary,J.A., Vosko,S.H., Jackson,K.A., Pederson,M.R., Singh,D.J. and Fiolhais,C. (1992) Atoms, molecules, solids, and surfaces: Applications of the generalized gradient approximation for exchange and correlation. *Phys. Rev. B*, **46**, 6671.
62. Vanderbilt,D. (1990) Soft self-consistent pseudopotentials in a generalized eigenvalue formalism. *Phys. Rev. B*, **41**, 7892.
63. Grimme,S. (2004) Accurate description of van der Waals complexes by density functional theory including empirical corrections. *J. Comput. Chem.*, **25**, 1463–1473.
64. Biswas,P.K. and Gogonea,V. (2005) A regularized and renormalized electrostatic coupling Hamiltonian for hybrid quantum-mechanical-molecular-mechanical calculations. *J. Chem. Phys.*, **123**, 164114.
65. Nosé,S. (1984) A molecular dynamics method for simulations in the canonical ensemble. *Mol. Phys.*, **52**, 255.
66. Hoover,W.G. (1985) Canonical dynamics: equilibrium phase-space distributions. *Phys. Rev. A*, **31**, 1695.
67. Tsvetkov,P.O., Devred,F. and Makarov,A.A. (2010) Thermodynamics of zinc binding to human S100A2. *Mol. Biol.*, **44**, 832–835.
68. Faralli,C., Pagliai,M., Cardini,G. and Schettino,V. (2007) The solvation dynamics of Na^+ and K^+ ions in liquid methanol. *Theor. Chem. Account*, **118**, 417–423.
69. Hancock,R.D., Siddons,C.J., Oscarson,K.A. and Reibenspies,J.M. (2004) The structure of the 11-coordinate barium complex of the pendant-donor macrocycle 1,4,7,10-tetrakis(carbamoylmethyl)-1,4,7,10-tetraazacyclododecane: an analysis of the coordination numbers of barium(II) in its complexes. *Inorg. Chim. Acta*, **357**, 723–727.
70. Hong,E.S., Yoon,H.-J., Kim,B., Yim,Y.-H., So,H.-Y. and Shin,S.K. (2010) Mass spectrometric studies of alkali metal ion binding on thrombin-binding aptamer DNA. *J. Am. Soc. Mass Spectrom.*, **21**, 1245–1255.
71. Shim,J.W., Tan,Q. and Gu,L.-Q. (2009) Single-molecule detection of folding and unfolding of the G-quadruplex aptamer in a nanopore nanocavity. *Nucleic Acids Res.*, **37**, 972–982.
72. Vairamani,M. and Gross,M.L. (2003) G-quadruplex formation of thrombin-binding aptamer detected by electrospray ionization mass spectrometry. *J. Am. Chem. Soc.*, **125**, 42–43.
73. Fadrná,E., Špačková,N., Štefl,R., Koča,J., Cheatham,T.E. and Šponer,J. (2004) Molecular dynamics simulations of guanine quadruplex loops: advances and force field limitations. *Biophys. J.*, **87**, 227–242.
74. Zacharias,M. (2000) Simulation of the structure and dynamics of nonhelical RNA motifs. *Curr. Opin. Struct. Biol.*, **10**, 311–317.
75. Perahia,D., Pullman,A. and Pullman,B. (1976) Cation-binding to biomolecules. *Theoret. Chim. Acta*, **42**, 23–31.
76. Turjanski,A.G., Hummer,G. and Gutkind,J.S. (2009) How mitogen-activated protein kinases recognize and phosphorylate their targets: a QM/MM study. *J. Am. Chem. Soc.*, **131**, 6141–6148.
77. Banás,P., Jurecka,P., Walter,N.G., Sponer,J. and Otyepka,M. (2009) Theoretical studies of RNA catalysis: Hybrid QM/MM methods and their comparison with MD and QM. *Methods*, **49**, 202–216.
78. Nagatoishi,S., Tanaka,Y. and Tsumoto,K. (2007) Circular dichroism spectra demonstrate formation of the thrombin-binding DNA aptamer G-quadruplex under

stabilizing-cation-deficient conditions. *Biochem. Biophys. Res. Commun.*, **352**, 812–817.
79. Fadrná,E., Špačková,N., Štefl,R., Koča,J., Cheatham,T.E. and Šponer,J. (2004) Molecular dynamics simulations of guanine quadruplex loops: advances and force field limitations. *Biophys. J.*, **87**, 227–242.
80. Cang,X., Šponer,J. and Cheatham,T.E. (2011) Explaining the varied glycosidic conformational, G-tract length and sequence preferences for anti-parallel G-quadruplexes. *Nucleic Acids Res.*, **39**, 4499–4512.
81. Zacharias,M. (2000) Simulation of the structure and dynamics of nonhelical RNA motifs. *Curr. Opin. Struct. Biol.*, **10**, 311–317.